7-2012

# Model of a Mechanical Clock Escapement

John Wagner
*Clemson University*, jwagner@clemson.edu

David Moline
*Clemson University*

Eugene Vold
*National Association of Watch and Clock Collectors*

# Model of a mechanical clock escapement

David Moline
*Department of Electrical Engineering, Clemson University, Clemson, South Carolina 29634*

John Wagner
*Department of Mechanical Engineering, Clemson University, Clemson, South Carolina 29634*

Eugene Volk
*National Association of Watch and Clock Collectors, Western Carolina Chapter #126, 636 Cherokee Terrace, Lake Toxaway, North Carolina 28747*

(Received 12 April 2011; accepted 9 April 2012)

The mechanical tower clock originated in Europe during the 14th century to sound hourly bells and later display hands on a dial. An important innovation was the escapement mechanism, which converts stored energy into oscillatory motion for fixed time intervals through the pendulum swing. Previous work has modeled the escapement mechanism in terms of inelastic and elastic collisions. We derive and experimentally verify a theoretical model in terms of impulsive differential equations for the Graham escapement mechanism in a Seth Thomas tower clock. The model offers insight into the clock's mechanical behavior and the functionality of the deadbeat escapement mechanism. 
[http://dx.doi.org/10.1119/1.4705517]

## I. INTRODUCTION

The mechanical tower clock emerged in Europe during the 14th century to mark the day's passage, initially through bells and later through dial hand displays.[1] Mechanical clocks use escapement mechanisms to convert stored energy from a weight or spring into the oscillatory motion of a pendulum or balance wheel. For instance, the escapement mechanism periodically (twice per period) applies an impulsive force to the pendulum near its equilibrium position to sustain its motion.[2] The evolution of clocks during the past seven centuries illustrates science and technology advancements with gear systems, materials, and escapement control. Bernstein has examined the history of feedback control systems starting with the mechanical clock escapement mechanism and continuing to the governor, aileron, and gyroscope.[3]

Headrick has reviewed the design of various clock escapement mechanisms, including the anchor (1657), Graham (1715), grasshopper (1722), pinwheel (1753), and Brocot (1860) mechanisms, and discussed the operation of the mechanical escapement mechanism to regulate speed.[4] Andronov *et al*. considered the dynamical behavior of oscillatory systems and analyzed the clock recoil escapement mechanism for inelastic conditions.[5] Kesteven established a framework to explore the relation between a clock's escapement mechanism and the period of the pendulum.[6] Lepschy *et al*. investigated a weight driven crown wheel escapement mechanism.[7] The interaction of the upper and lower pallets with the crown wheel teeth was assumed to be both inelastic and elastic. The dynamics were treated using a hybrid continuous-discrete model. Roup and Bernstein studied a verge escapement and foliot clock.[8] The verge escapement features a circular wheel (crown) with sawtooth shaped teeth which engage a vertical rod (verge) with two pallets (metal plates) as it rotates to give an impulse to an attached pendulum.[9] Their analysis used differential equations subjected to impulse effects to analyze the escapement mechanism's motion with different values of the coefficient of restitution. Roup *et al*. also used impulsive differential equations and Poincare maps to demonstrate a limit cycle of a verge and foliot escapement mechanism.[10]

The availability of a large tower clock at Clemson University enables us to compare our observations with a nonlinear model that we will describe in the following. A weight driven Seth Thomas tower clock in Fig. 1 was installed at Clemson in 1904 to display the time and strike the hour on a large bell. The suspension spring supports a wooden pendulum rod with a concentrated metal bob which interfaces to a Graham deadbeat escapement mechanism through the crutch arm attached to the verge arbor mechanical linkage.[11] The escape wheel in a deadbeat escapement does not recoil when an escape wheel tooth drops onto the pallet or when the verge moves.[9] The two pallets connect to the host shaft, or arbor, which moves the crutch (typically a vertical shaft with an attached pin or forked opening) which transmits the escapement power to the pendulum. The wheels and pinions in the clock's gear train are responsible for time keeping and include four arbors, three gear interfaces, and the escape wheel. The final wheel in the time train, which interfaces with the escapement pallets, is the escape wheel. An arbor, or axle, hosts the toothed wheel or gear, which transmits motion within the clock. The minute hand is driven by the second arbor through bevel gears; the hour hand displays a 1:12 ratio with the minute hand. The strike train, or mechanical elements responsible for the bell strike functionality of the clock, contains a cam driven interface from the time train side and a cam with a snail shell profile to regulate bell strikes, with a rack/lever powered by a second weight wheel.

In this article, we will derive a nonlinear dynamical model for the weight driven Graham escapement clock and test the model experimentally. Section II presents a theoretical model for the clock escapement mechanism and accompanying time side gear dynamics. The escape wheel and Graham deadbeat escapement instrumentation is reviewed in Sec. III. In Sec. IV, experimental and numerical results are discussed for the tower clock at Clemson University. A summary is offered in Sec. V.

## II. CLOCK MODEL

The Seth Thomas tower clock time train consists of the weight driven assembled wheels and pinions which drive the

  

Fig. 1. 1905 Seth Thomas tower clock at Clemson University mounted on a pedestal with pendulum and clock face assembly.

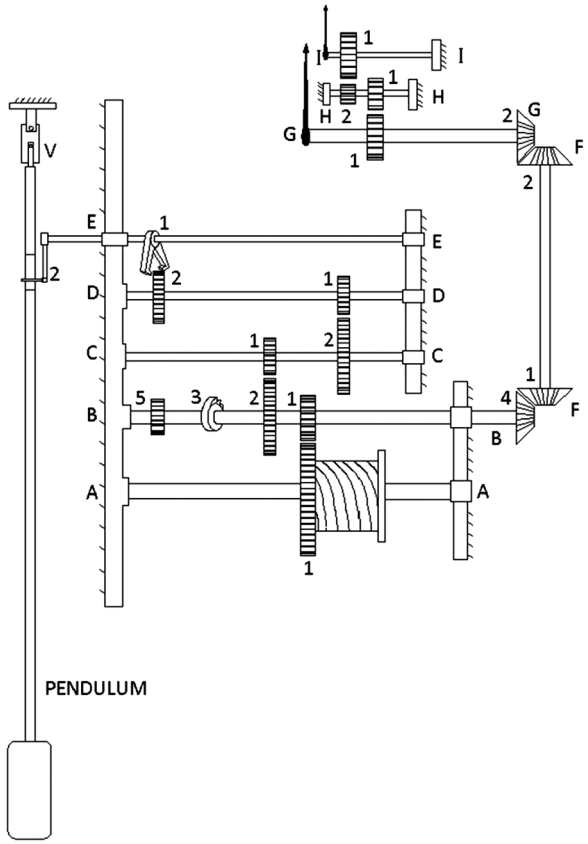


Fig. 2. Seth Thomas time keeping clockworks with definitions of the wheels and arbors.

Graham deadbeat escapement and pendulum.[12] A diagram of the clock time train is displayed in Fig. 2. The great wheel arbor (A) contains the drum, or metal barrel, around which a twisted metal line is wound. A series of cylindrical weights are attached to the line to create a counter-clockwise torque to drive the motion works when viewed from the clock's pendulum side. At arbor A, wheel 1 interfaces with the input pinion and small gear 1 on arbor B to transmit the weight induced drive orque. Arbor B makes one revolution every 60 min and drives the time display through bevel gear 4. The vertical arbor F features identical bevel gears 1 and 2 which interface, respectively, with arbors B and G using a one-to-one ratio. The minute motion is transmitted to the clock's distant four dials using leading-off-rods, which are long metal rods with attached bevel gears. Only one dial and arbor G will be considered for simplicity. Bevel gear 2 on arbor G meshes with bevel gear 2 on arbor F to drive both the minute arbor pinion 1 and the minute hand. The mechanical gearing on arbors G, H, and I provide a 12:1 reduction to convert the minute hand motion to a 12 h rotation for display on arbor I. In the actual clock, arbors G and I are concentric to allow a traditional time display.

The rotational speed of arbor B is regulated by the oscillatory motion of the pallet arbor of the verge escapement. On arbor B, wheel 2 meshes with pinion 1 on the intermediate arbor C. Wheel 5 and cam 3 on arbor B control the bell strike process. Wheel 2 on arbor C meshes with pinion 1 on arbor D which hosts escape wheel 2. On arbor E, verge 1 repeatedly interfaces with the escape wheel teeth. Specifically, two hardened steel pallets are struck by the escape wheel teeth, thus transmitting the rotational motion to the verge. At the end of arbor E, crutch 2 gives an impulse to the pendulum at each beat to maintain oscillatory motion. This mechanical coupling between the verge, crutch pin, and pendulum ensures that the pendulum receives periodic impulses based on the verge motion. The compound pendulum features a long wooden rod with a metal cylindrical bob of height $h_{\text{bob}}$ and diameter $d_{\text{bob}}$. The pendulum is hung from the tower clock assembly by a flat suspension spring (V) to achieve a beat (time of travel) of 1.5 s. The arbor, gear, symbol, description, number of teeth, outer diameter, and length for each component are listed in Table I.

### A. Time side gear train

The torque $T_{A_1}$ on the great wheel, $A_1$, arises from the external weight of the suspended steel cable, which acts on the barrel so that $T_{A_1} = m_A g r_A$, where $m_A$ and $r_A$ represent the external hung mass and barrel radius, respectively. The input torque is reduced by various gear interfaces to power the clock display and escape wheel interaction with the deadbeat escapement. If the gears are assumed to be ideal, then the torque and rotational speed relation is $T_{D_2} = (1/R_t)T_{A_1}$ and $\omega_{D_2} = R_t \omega_{A_1}$ with the time works train ratio, $R_t$, given by

$$R_t = \left(\frac{\phi_{A_1}}{\phi_{B_1}}\right)\left(\frac{\phi_{B_2}}{\phi_{C_1}}\right)\left(\frac{\phi_{C_2}}{\phi_{D_1}}\right). \tag{1}$$

In these expressions, $T_{D_2}, \omega_{D_2}$, and $\omega_{A_1}$ denote the escape wheel torque, escape wheel rotational speed, and great wheel angular speed, respectively. The quantities $\phi_{A_1}, \phi_{B_1}, \phi_{B_2}, \phi_{C_1}, \phi_{C_2}$, and $\phi_{D_1}$ represent the diameters of the great wheel,

Table I. Nomenclature of the tower clock time side gear train and corresponding values with the number of wheel teeth, $N$, wheel diameter, $\phi$, and shaft length, $L$. Arbor E has two different diameters with their corresponding shaft lengths in parentheses when considered from the clock's back to front plates.

| Arbor | Gear | Symbol | Description | $N$ | $\phi$ (mm) | $L$ (mm) |
|---|---|---|---|---|---|---|
| A | | | Arbor A | | 25.4 | 460.38 |
| A | 1 | $A_1$ | Great wheel | 120 | 314.9 | |
| B | | | Arbor B | | 19.05 | 384.18 |
| B | 1 | $B_1$ | Input pinion | 20 | 55.35 | |
| B | 2 | $B_2$ | arbor C Wheel | 112 | 222.7 | |
| B | 3 | $B_3$ | strike side Cam | — | — | |
| B | 4 | $B_4$ | Bevel gear | 40 | 106.7 | |
| B | 5 | $B_5$ | pinion Strike side | 13 | 24.04 | |
| C | | | Arbor C | | 109.22 | 225.43 |
| C | 1 | $C_1$ | arbor C Pinion | 14 | 28.96 | |
| C | 2 | $C_2$ | Drive Wheel $D_1$ | 90 | 129.0 | |
| D | | | Arbor D | | 12.95 | 225.43 |
| D | 1 | $D_1$ | Arbor D pinon | 12 | 42.33 | |
| D | 2 | $D_2$ | Escape Wheel | 20 | 95.25 | |
| E | | | Arbor E | | 12.80 (195.00), 8.00 (75.00) | 270.00 |
| E | 1 | $E_1$ | Verge | — | — | |
| E | 2 | $E_2$ | Crutch assembly | — | — | |
| F | 1 | $F_1$ | Bevel gear | 40 | 106.7 | |
| F | 2 | $F_2$ | Bevel gear | 40 | 106.7 | |
| G | 1 | $G_1$ | Minute arbor pin | 15 | 26.62 | |
| G | 2 | $G_2$ | Bevel gear | 40 | 106.7 | |
| H | 1 | $H_1$ | Motion wheel | 45 | 14.06 | |
| H | 2 | $H_2$ | Motion wheel | 12 | 21.33 | |
| I | 1 | $I_1$ | Hour hand pin | 48 | 78.90 | |

arbor B pinion, wheel two on arbor B, arbor C pinion, wheel two on arbor C, and arbor D pinion.

### B. Escape wheel and verge interface

The interaction between the escape wheel and verge is important, given the mechanical feedback controller functionality of these two components in the Graham deadbeat escapement. Figure 3 displays this interaction with the important dimensions. When the clock is running, the crutch transmits power from the escapement to the pendulum so that the latter swings through the angle $\theta_p$. For the purposes of this paper, the pendulum, crutch, and verge are modeled as one part rotating about $O$. This motion causes the verge pallets to alternately block the free rotation of the escape wheel, which rotates about the escape wheel arbor $O'$ shown in Fig. 3, whereupon the escape wheel tooth lands on the lock face of the pallet. The lock faces are curved, with radii $r_p$ and $r_p + h$, respectively, about $O$, which results in no additional motion of the escape wheel, while the crutch continues to move. In escapement designs that lack curved lock faces, the pallet forces the escape wheel to move backward slightly, or recoil, while sliding on the lock face. This behavior wastes energy and excessively perturbs the pendulum, affecting the time-keeping accuracy. The absence of recoil is a key feature of the deadbeat mechanism.

When the crutch reverses direction and withdraws the pallet, the escape wheel tooth slides onto the angled impulse face of the pallet, allowing the drive torque from the drive weight to rotate the escape wheel and give an impulsive force to the pendulum. The angles $\beta_1$ and $\beta_2$ are chosen to maximize the efficiency of the impulse. When the escape wheel tooth leaves the impulse face, the wheel rotates freely under the drive torque alone until another escape wheel tooth impacts the lock face of the opposite pallet, which is designed to be in a position to lock it. (This impact is the audible "tic" of the clock in motion; the impact on the left and right pallets will often sound different, and hence a "tic" and "toc" sound will be noticed). The escape wheel rotates 9° while moving from the locked position on the lock face of the pallet to lock on the other pallet lock face. Specifically, it moves 7° while impulsing the pendulum and 2° in free spin.

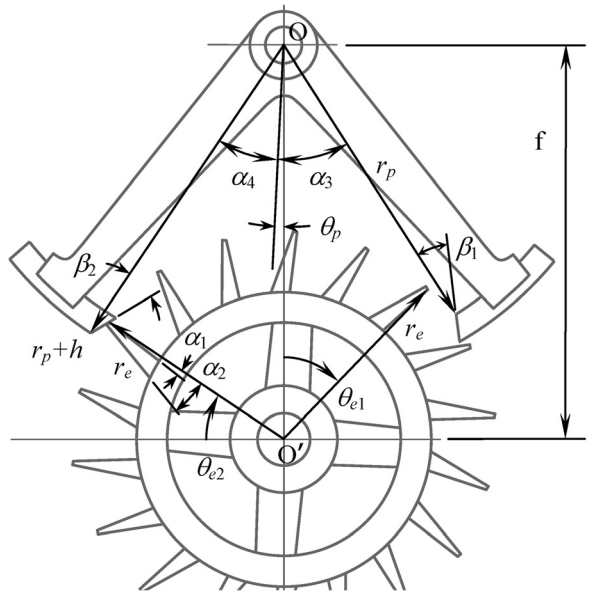


Fig. 3. Deadbeat escapement showing the escape wheel and verge with twin pallet geometry as viewed from the front of the tower clock.

### C. Crutch and escape wheel dynamics

We have explained the defining feature of the Graham deadbeat escapement—the interaction of the verge and escape wheel. A simulation of this mechanism must accurately model this interaction, and especially address the intermittent contact between these two parts which create the time keeping motion. The equations of motion used to simulate the Graham deadbeat mechanism motion will next be discussed.

The system equations of motion were formulated using Haug's method.[13] This method allows us to write the equations of motion directly from information obtained from a kinematic analysis of the system, without formulating and subsequently differentiating the Langrangian. In this instance, the equation of motion was written with the following structure:

$$G^T M G \ddot{\theta} = S^T f. \tag{2}$$

The system degrees of freedom are contained in the vector $\theta$ taken to be the verge and escape wheel angles, $\theta_p$ and $\theta_e$. $M$ is a diagonal matrix of the mass and mass moments of inertia of the moving parts in the system, and $f$ is a vector of forces and includes the gravitational forces acting on the pendulum and drive weight, and the contact forces between the escape wheel teeth and verge pallets. The matrices $S$ and $G$ come from the kinematic analysis of the mechanism as needed to

apply Haug's method. Further explanation of the matrices $M$, $G$, and $S$ as well as the system forces is given in the remainder of this section.

The mass matrix $M$ includes the various arbors and attached parts of the clock mechanism, in addition to the pendulum components and the drive weight

$$M = \mathrm{diag}\begin{pmatrix} J_E + J_{E_1} + J_{E_2} \\ \frac{1}{3} m_{\mathrm{rod}} L_{\mathrm{rod}}^2 \\ \frac{1}{12} m_{\mathrm{bob}} h_{\mathrm{bob}}^2 + \frac{1}{4} m_{\mathrm{bob}} d_{\mathrm{bob}}^2 + m_{\mathrm{bob}} \left( L_{\mathrm{bob}} + \frac{1}{2} h_{\mathrm{bob}} \right)^2 \\ J_D + J_{D_1} + J_{D_2} \\ J_D + J_{D_1} + J_{D_2} \\ J_B + J_{B_1} + J_{B_2} + J_{B_4} \\ J_A + J_{A_1} \\ m_A \end{pmatrix}, \tag{3}$$

where $J$ is the moment of inertia and $G$ is defined such that $G\dot{\theta}$ is a vector of linear and angular velocities of the masses in the system so that $MG\dot{\theta}$ is the vector of the linear and angular momentum of each mass in the system. For example, the first element of $MG\dot{\theta}$ is the total angular momentum of arbor $E$ with the verge and crutch attached to it in Fig. 2, the second element is the angular momentum of the wooden pendulum shaft, and the third element is that of the pendulum bob. In addition to $R_t$ from Eq. (1) readers will recognize in $G$ other ratios of the gear diameters in the time side geartrain, giving the angular velocity of each arbor (and gears) in terms of the angular speed of the escape wheel, $\theta_e$. Note that $(r_A/R_t)\,\theta_e$ is the linear velocity of the falling drive weight.

$$G = \begin{bmatrix} 1 & 1 & 1 & 0 & 0 & 0 & 0 & 0 \\ 0 & 0 & 0 & 1 & \phi_{D_1}/\phi_{C_2} & (\phi_{C_1}/\phi_{B_2})(\phi_{D_1}/\phi_{C_2}) & 1/R_t & r_A/R_t \end{bmatrix}^T. \tag{4}$$

The term $G^T M G$ is also the effective mass matrix of the system. This quantity reduces to a $2 \times 2$ matrix with only two non-zero elements, both on the diagonal, thus meaning that the two differential equations in Eq. (2) are uncoupled.

It is useful to examine the contributions to the total rotational inertia in each equation of motion. It is expected that the pendulum's bob inertia dominates the pendulum equation of motion (it accounts for 99.3% of the rotational inertia). The time side geartrain ratios are such that 94% and 5% of the total rotational inertia comes from arbors $D$ and $C$ (and their components), respectively, despite the large diameter of the great wheel barrel and the size of the applied external weight.

Although $G^T$ and $M$ are constant, or time-invariant, in this system (not always the case, in general), the matrix $S$ depends on the degrees of freedom, $\theta_p$ and $\theta_e$, due to the geometry of the escape wheel teeth and verge pallets.

The quantity $S$ is chosen such that $S\dot{\theta}$ is the vector of relative velocities across the force generating elements in the system, that is, the relative motion along the line of action of each force in the system. The term $S^T f$ is a vector of generalized forces obtained by the Lagrangian method: $S^T$ is a matrix of virtual displacements which determines the contribution of each force in $f$ to the individual equations of motion. $G^T$ in Eq. (2) performs a similar function, because $MG\ddot{\theta}$ is a vector of inertial forces.

To derive $S$, we identify the forces to be modeled in the system and calculate the motion of the points where these forces act, for example, the vertical translation of a part moving in a gravitational field or the deflection of a compliant element. With expressions for these motions in hand, we then differentiate them with respect to the degrees of freedom and assemble the matrix; that is, $S$ is the Jacobian matrix of these expressions. The discussion of this process for determining $S$ is given in the following.

There are ten forces modeled in the system. Two are gravitational loads on the pendulum and the drive weight; the remainders are forces associated with the contact of an escape wheel tooth with either the left or right verge pallet as shown in Fig. 3. That is, an escape wheel tooth may touch a pallet face on either of two surfaces, the lock face or the impulse face. This normal contact force will have an associated friction force when the escape wheel tooth slides along the face. Thus, there are two possible normal loads on the right pallet, with two possible friction forces, and the same for the left pallet, for a total of eight contact and friction forces.

The contact and friction forces are calculated using the geometry shown in Fig. 4, which we use as an example. The large gap between the escape wheel tooth and the verge pallet is exaggerated. Four calculated quantities are shown, $d_{\mathrm{lock}}, e_{\mathrm{lock}}, d_{\mathrm{impulse}}$, and $e_{\mathrm{impulse}}$, which give the position of the escape wheel tooth tip $B$ relative to the verge pallet corner $A$. The corner $A$ is the boundary of the two faces of the pallet where the escape wheel tooth tip $B$ might contact the pallet.[14] The quantities $d_{\mathrm{lock}}$ and $d_{\mathrm{impulse}}$ are measures of the radial distance (along a radius from $O$) and the perpendicular distance, respectively, from these two faces to $B$. As shown, $d_{\mathrm{lock}}$ is taken to be positive, and $d_{\mathrm{impulse}}$ is negative. The contact forces acting on $B$ and these surfaces are calculated as

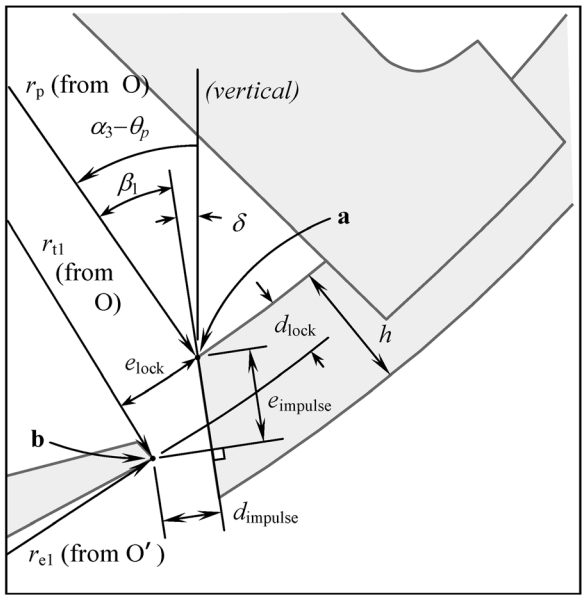


Fig. 4. Detailed view of the interaction of the escape wheel teeth and right pallet on the verge.

the product of the linear stiffness, $k_c$, and the quantities $d_{\text{impulse}}$ and $d_{\text{lock}}$.

If $d_{\text{impulse}}$ or $d_{\text{lock}}$ is less than zero, the corresponding force is set to zero (no contact with the surface). Because both forces cannot act at the same time in the event that both are positive (an allowable condition since the two degrees of freedom are independent), the quantities $e_{\text{lock}}$ and $e_{\text{impulse}}$ are also calculated and used to determine which force should be zeroed and which should remain as calculated. These two quantities give the distance from corner $A$ on the pallet to the contact point where the normal force should act along the lock face or impulse face, respectively; if one is negative, it is impossible that tip $B$ is engaging that surface of the pallet. (The arc of the lock face and line of the impulse face are extrapolated as necessary for the calculation.) In Fig. 4, $e_{\text{lock}}$ is defined to be negative and $e_{\text{impulse}}$ is positive as shown. Therefore, only a force acting on the impulse face should be admitted. However, this normal force is zero because the normal distance, $d_{\text{impulse}}$, is negative: tip $B$ is not touching the pallet impulse face.

Figure 5 summarizes the decision logic to zero a force or allow it to remain enabled (that is, as calculated). From Fig. 4, because $d_{\text{lock}}$ is positive, a contact or normal force on the lock face is possible, but because $e_{\text{lock}}$ is negative, this normal force is zeroed. The next decision block also fails, as discussed, and no contact forces act between the pallet and escape wheel tooth. This case is what we expect from the configuration shown: the two parts are not touching. The logic in Fig. 5 includes two other tests. The test for $d_{\text{lock}} < h$ determines that tip $B$ has not already swept past the pallet impulse face. The comparison of $e_{\text{lock}}$ and $e_{\text{impulse}}$ in each decision block establishes priority between the lock and impulse normal forces in the event that both are possible; for example, $d_{\text{lock}}, e_{\text{lock}}, d_{\text{impulse}}$, and $e_{\text{impulse}}$ are all positive. This event can occur because the contact is modeled as an elastic one: the forces keep the two parts in motion relative to each other, but it is possible for tip $B$ to overlap the verge pallet. In reality, there would be some minute deflection of the contact surfaces and the escape wheel tooth.

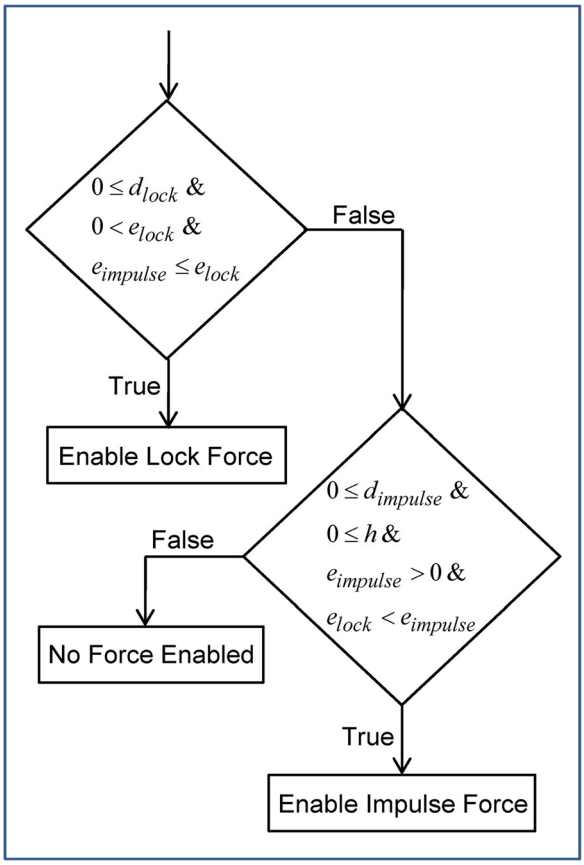


Fig. 5. Logic for the implementation of the lock force and impulse force at the escape wheel and pallet interfaces.

Because not all the energy is conserved during this elastic interaction, a linear damping force is also added to the normal load, for example, $F_{c_{\text{lock}}} = (k_c d_{\text{lock}} + b_c \dot{d}_{\text{lock}})$ and $F_{c_{\text{impulse}}} = (k_c d_{\text{impulse}} + b_c \dot{d}_{\text{impulse}})$. There is also a loss associated with friction as the escape wheel tooth slides on either pallet face, which is calculated as the product of a coefficient of friction $\mu$, and the normal load and the sign is corrected to act against the relative motion, for example, $\mu F_{c_{\text{lock}}} sgn(\dot{e}_{\text{lock}})$ and $\mu F_{c_{\text{impulse}}} sgn(\dot{e}_{\text{impulse}})$.

In addition to being used to calculate the contact forces, the quantities $d_{\text{lock}}, e_{\text{lock}}, d_{\text{impulse}}$, and $e_{\text{impulse}}$ for the left and right verge pallets, and expressions for the motion of the drive weight and pendulum against gravity are used to formulate $S$ as the Jacobian matrix of these quantities as

$$S = \begin{pmatrix} \nabla d_{\text{lock}_{\text{left}}} \\ \nabla e_{\text{lock}_{\text{left}}} \\ \nabla d_{\text{impulse}_{\text{left}}} \\ \nabla e_{\text{impulse}_{\text{left}}} \\ \nabla d_{\text{lock}_{\text{right}}} \\ \nabla e_{\text{lock}_{\text{right}}} \\ \nabla d_{\text{impulse}_{\text{right}}} \\ \nabla e_{\text{impulse}_{\text{right}}} \\ \nabla (r_A/R_t)\theta_e \\ \nabla L_{p,cg} \sin(\theta_p) \end{pmatrix}^T . \tag{5}$$

The last two entries in Eq. (5) are the vertical motion of the centers of gravity of the drive weight and pendulum system, respectively.

### D. Clock hand motion

The angular speed of the minute and hour hands, $\omega_m$ and $\omega_h$, on each clock face depends on the time gear train motion such that $\omega_m = (1/R_m)\omega_{D_2}$,

$$R_m = (\phi_{B_2}/\phi_{C_1})(\phi_{C_2}/\phi_{D_1})(\phi_{F_1}/\phi_{B_4})(\phi_{G_2}/\phi_{F_2}), \qquad (6)$$

with $\omega_h = (1/R_h)\omega_m$, and $R_h = \left(\frac{\phi_{H_1}}{\phi_{G_1}}\right)\left(\frac{\phi_{I_1}}{\phi_{H_2}}\right)$. In terms of the minute arbor to hands display mechanical linkage, the location of the minute arbor is at least one (intermediate) shaft removed from the escape wheel arbor, which hosts the escape wheel and subsequent verge interface. For typical applications (the current tower clock does not have hands or leading-off-rods attached and they have not been considered in the model), the four sets of hands exert a torque on the time train. Specifically, the applied torque continually varies as the minute hands rotate through a 60 min period. As discussed in Ref. 15, the clock movement receives assistance (hindrance) from the weight of the minute hand between 12 a.m. and 6 a.m. (6 p.m. to 12 p.m.). The hour hand likely has a similar, but minor effect due to being shorter, lighter, and slower (1/12 geared speed) than the minute hand. Consequently, these hands may be counterweighted and/or constructed of lighter materials such as wood or aluminum. However, the pendulum's inertia and the escapement mechanism generally minimize the net effect of torque variations.

In terms of overall clock timekeeping accuracy, the most significant effect is variations in the pendulum's swing due to changes in the temperature, humidity, and torque applied to the escapement.[16,17]

## III. CLOCK ESCAPEMENT INSTRUMENTATION

The motion of the escape wheel and deadbeat escapement was measured using separate instrumentation systems. Two miniature solid state rate gyroscopes were directly attached to the verge and pendulum. The Analog Devices ADXRS150 $\pm 150°/s$ single chip yaw rate gyro with signal conditioning was selected because it produces a voltage dependent on the normal axis angular speed.[18] The filtered angular speed and acceleration signals were measured by a 12-bit National Instruments DAQ card, sampling at 200 Hz. A horology specific high precision timer was also attached near the escapement using an acoustic sensor to validate the measured period and identify the accompanying rate error. The MicroSet electronic system can measure the clock's beat to within a millionth of a second.[19]

## IV. NUMERICAL AND EXPERIMENTAL RESULTS

The description of the Graham deadbeat escapement and Seth Thomas motion works were validated using results from the Clemson University tower clock. The model was simulated in MATLAB/SIMULINK and compared with experimental results using the instrumentation described in Sec. III. The arbor and wheel inertias were calculated based on the clock's materials and geometry. The values for the clock model parameters are listed in Table II and allow the gear train-escapement-pendulum system to be simulated by interested readers.

Select experimental results for the escape wheel and clock escapement are shown in Figs. 6–9. The graphs show the angular position obtained by numerical integration. The sensor output for the escape wheel acceleration saturated at $2000°/s^2$ and was not useable. Instead, a numerical model of the differentiator and filter was implemented to reproduce the signal from the measured angular rate. The analog and numerical filters introduced a 6.5 ms lag in the measurements in addition to attenuation of transient events. Positive angles and rates correspond to the clockwise rotation of either the escape wheel or verge when viewed from the clock's front. The sensors were attached to the front surface of these two components. The Seth Thomas tower clock escapement with pendulum was designed to operate at a period of 3 s or 1.50 s per beat (2400 beats per hour). The clock operated at 1.5014 beats per second or 30 s per day error rate as measured using the MicroSet timer during a 20 min interval.

Table II. Summary of clock tower parameter values.

| Symbol | Value | Symbol | Value |
|---|---|---|---|
| $b_c$ | 3 Ns/mm | $L_{\text{bob}}$ | $2.0193 \times 10^2$ cm |
| $d_{\text{bob}}$ | 16.51 cm | $L_{\text{rod}}$ | $2.3812 \times 10^2$ cm |
| F | 90.8050 mm | $m_A$ | 45.4 kg |
| G | 9.81 m/s$^2$ | $m_{\text{bob}}$ | 61.2 kg |
| H | 5.9944 mm | $m_{\text{rod}}$ | 1.1 kg |
| $h_{\text{bob}}$ | 36.195 cm | $r_A$ | 10 cm |
| $J_A$ | $1.4806 \times 10^{-4}$ kg m$^2$ | $r_e$ | 47.7266 mm |
| $J_{A_1}$ | $1.1047 \times 10^{-1}$ kg m$^2$ | $R_h$ | 12 |
| $J_B$ | $3.9093 \times 10^{-5}$ kg m$^2$ | $R_m$ | 60 |
| $J_{B_1}$ | $7.0790 \times 10^{-5}$ kg m$^2$ | $r_p$ | 74.4220 mm |
| $J_{B_2}$ | $5.6248 \times 10^{-3}$ kg m$^2$ | $R_t$ | 360 |
| $J_{B_4}$ | $1.0402 \times 10^{-3}$ kg m$^2$ | T | 3.00 s |
| $J_C$ | $2.47863 \times 10^{-6}$ kg m$^2$ | $T_{A_1}$ | 1.127 Nm |
| $J_{C_1}$ | $5.3035 \times 10^{-6}$ kg m$^2$ | $w_{A_1}$ | 15.875 mm |
| $J_{C_2}$ | $1.2449 \times 10^{-3}$ kg m$^2$ | $w_{B_1}$ | 10.668 mm |
| $J_D$ | $4.9046 \times 10^{-6}$ kg m$^2$ | $w_{B_2}$ | 7.747 mm |
| $J_{D_1}$ | $1.0698 \times 10^{-6}$ kg m$^2$ | $w_{B_4}$ | 11.684 mm |
| $J_{D_2}$ | $6.8011 \times 10^{-4}$ kg m$^2$ | $w_{C_1}$ | 10.668 mm |
| $J_E$ | $4.2817 \times 10^{-6}$ kg m$^2$ | $w_{C_2}$ | 6.350 mm |
| $J_{E_1}$ | $4.446 \times 10^{-3}$ kg m$^2$ | $w_{D_1}$ | 10.668 mm |
| $J_{E_2}$ | $3.145 \times 10^{-4}$ kg m$^2$ | $w_{D_2}$ | 11.684 mm |
| $J_P$ | $2.9780 \times 10^2$ kg m$^2$ | $\rho_{\text{brass}}$ | $8.575 \times 10^3$ kg/m$^3$ |
| $J_{\text{bob}}$ | $2.5032 \times 10^2$ kg m$^2$ | $\rho_{\text{steel}}$ | $7.870 \times 10^3$ kg/m$^3$ |
| $J_{\text{rod}}$ | 1.7750 kg m$^2$ | $\rho_{\text{wood}}$ | 900 kg/m$^3$ |
| $k_c$ | 100 N/mm | $\mu$ | 0.01 |

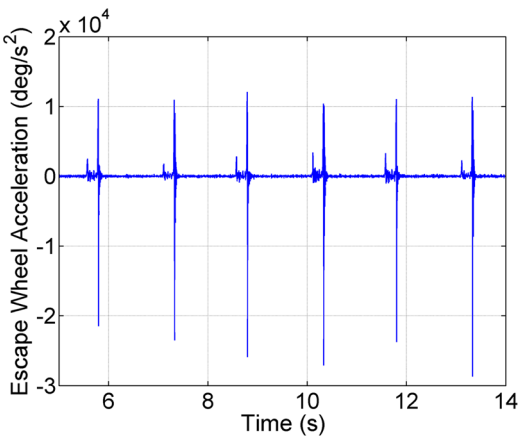


Fig. 6. Experimental results for the escape wheel angular acceleration (deg/s$^2$) over three periods showing left and right pallet impulse events.

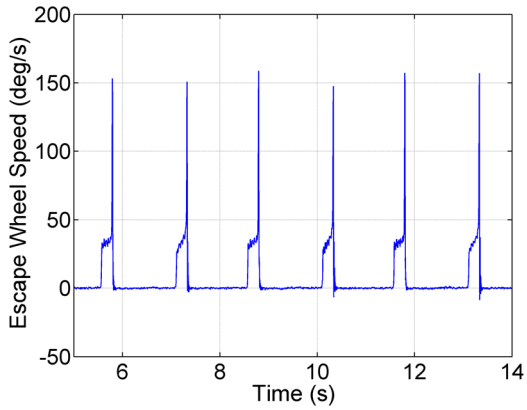


Fig. 7. Experimental results for the escape wheel angular speed (deg/sec) over three periods with the lock, impulse, and free spin sequence. Note the subtle differences between the left and right pallet interactions with the escape wheel.

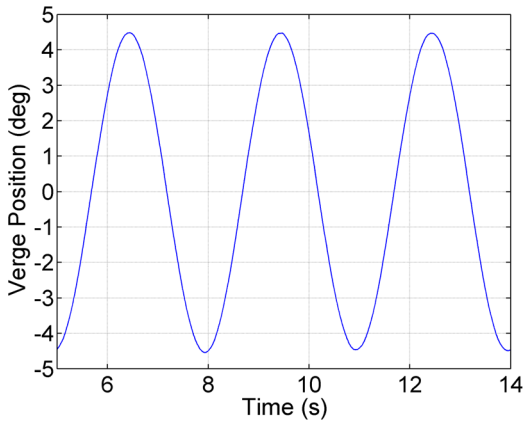


Fig. 9. Experimental results for the verge angular position (deg) over three periods which also corresponds to the pendulum harmonic motion due to the verge crutch pin to pendulum rod connection.

The escape wheel acceleration data in Fig. 6 displays small spikes of about $2500°/s^2$, followed 0.20 s later by larger spikes on the order of $10000°/s^2$. These are the start and finish, respectively, of each impulse to the pendulum, during which time the escape wheel rotates at about 35°/s (see Fig. 7). Some acceleration is evident during the impulse, and this acceleration is greater at the right pallet than the left as shown at $t = 7.1$ s and $t = 10.1$ s, respectively. At the end of each impulse, for example $t = 7.3$ s, the escape wheel is free of the given verge pallet and accelerates for 10 ms, reaching an angular speed of about 150°/s before impacting the other verge pallet, causing the spikes in these two graphs. Between impulses, the escape wheel shows no recoil as evident by the constant angular positions in Fig. 8. The escape wheel advances approximately 9.0° per impulse. The equal spacing shown on these three plots between each impulse indicates that this clock is "in beat" or symmetric in its swing. The pendulum motion in Fig. 9 is smooth and reflects the expected harmonic motion with a period of 3.0 s, rotational speed of ±9.5°/s, and rotational oscillations of ±4.5°.

The numerical results for the time side gear train, escape wheel and verge, and pendulum model are displayed in Figs. 10 and 11. The angular acceleration of the escape wheel in Fig. 10 compares favorably with the experimental results shown in Fig. 6 in terms of the amplitude and spike timing. The escape wheel speed in Fig. 11 displays a free spin profile similar to Fig. 7 for the impulse, which briefly occurs when the pallets do not interact with the escape wheel teeth. The escape wheel positions were nearly identical with respect to the amplitude and duration of the stair steps. Overall, the escapement descriptions of the lock, impact, and "no force" (escape wheel free spin) regimes are accurately described by our model. The simulated harmonic motion of the combined verge with pallets, arbor, crutch, and pendulum also agrees well with the experimental data. The period of the verge is 2.98 s, an error of 0.7%. Figures 10 and 11 lack the sensor noise and do not include the impact features observed in Figs. 6 and 7. The absence of these features may be attributed to sensor installation and/or to the motion of clock parts which were not included in the model.

Obtaining excellent agreement with the experimental results, especially regarding the escape wheel dynamics, required the careful tuning of the model by parameter verification. Accurate knowledge of the parameters shown in Fig. 3 is required and errors as small as 0.01 mm for the dimensions $r_p$ and $f$ affects the characteristic response. Because this accuracy was not easily attained, it was necessary to explore the effects of uncertainty in the measurements until satisfactory results were obtained.

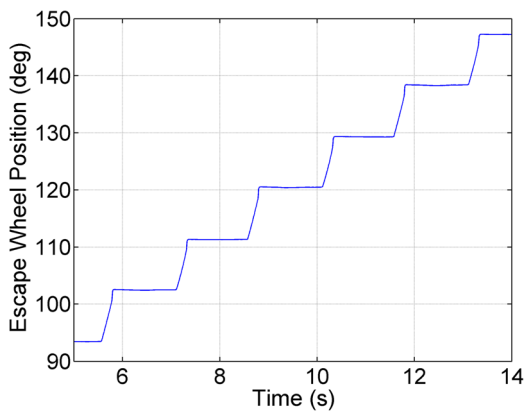


Fig. 8. Experimental results for the escape wheel angular position (deg) over three periods showing two incremental advancements per minute of the escape wheel.

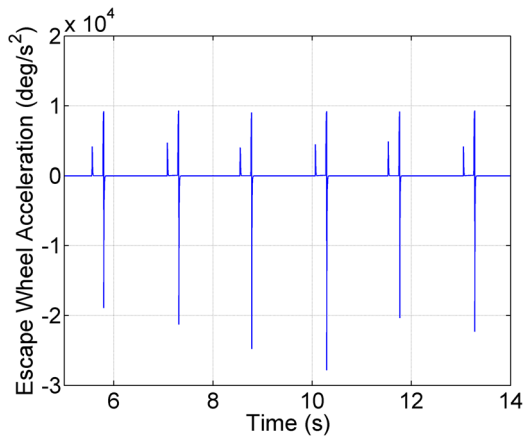


Fig. 10. The numerical results for the escape wheel angular acceleration ($deg/s^2$) over three periods closely match the experimental results in Fig. 6.

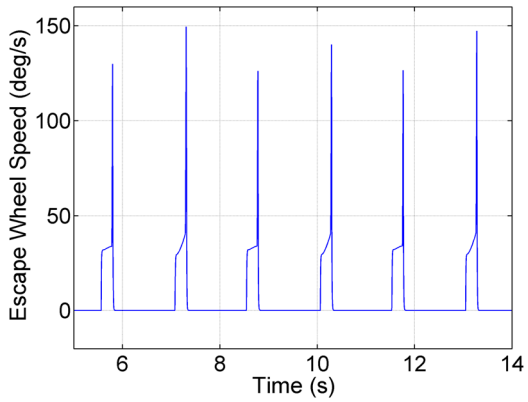


Fig. 11. The numerical results for the escape wheel angular speed (deg/sec) over three periods favorably correspond in terms of the amplitude and time interval to the experimental results in Fig. 7.

## V. SUMMARY

Mechanical tower clocks with Graham deadbeat escapement mechanisms have maintained time for over 290 years. These mechanisms convert potential energy into oscillatory motion to display the passage of time and strike bells. We derived a nonlinear model to describe the train motion, including the escape wheel and integrated escapement mechanism with an attached pendulum. Representative data were presented, and overall agreement of the numerical and experimental results was realized. The tower clock offers an excellent example of fundamental scientific principles and engineering elegance that has served society well for centuries.

## ACKNOWLEDGMENTS

The authors wish to thank the National Association of Watch & Clock Collectors (NAWCC) Western Carolinas Chapter No. 126 for restoring the clock, and Clemson University faculty and students M. Daqaq, A. Jagarwal, and J. Savitsky for their contributions to the clock analysis and manuscript. The authors also greatly appreciate the insightful comments from the reviewers.

[1]D. Boorstin, *A History of Man's Search to Know His World and Himself* (Random House, New York, 1983).
[2]A. L. Rawlings, *The Science of Clocks and Watches*, 3rd ed. (British Horological Institute, Upton, England, 1993).
[3]D. Bernstein, "Feedback control: An invisible thread in the history of technology," IEEE Control Syst. Mag. **22**(2), 53–68 (2002).
[4]M. V. Headrick, "Origin and evolution of the anchor clock escapement," IEEE Control Syst. Mag. **22**(2), 41–52 (2002).
[5]A. A. Andronov, A. A. Vitt, and S. E. Khaikin, *Theory of Oscillators*, edited by W. Fishwick and translated by F. Immirzi (Addison-Wesley, Reading, MA, 1966).
[6]M. Kesteven, "On the mathematical theory of clock escapements," Am. J. Phys. **46**(2), 125–129 (1978).
[7]A. Lepschy, G. Mian, and U. Viaro, "Feedback control in ancient water and mechanical clocks," IEEE Trans. Educ. **35**(1), 3–10 (1992).
[8]A. V. Roup and D. S. Bernstein, "On the dynamics of the escapement mechanism of a mechanical clock," in *Proceedings of the 38th Conference on Decision and Control*, IEEE Control System Society, Vol. 3, Phoenix, AZ, December 1999, pp. 2599–2604.
[9]D. de Carle, *Watch and Clock Encyclopedia* (Bonanza Books, New York, 1977).
[10]A. V. Roup, D. S. Bernstein, S. G. Nersesov, W. M. Haddad, and V. Chellaboina, "Limit cycle analysis of the verge and foliot clock escapement using impulsive differential equations and Poincare maps," Int. J. Control **76**(17), 1685–1698 (2003).
[11]L. Penman, *Practical Clock Escapements* (ClockWorks, West Sacramento, CA, 1998).
[12]J. Wagner, C. Huey, K. Knaub, E. Volk, and A. Jagarwal, "Modeling and analysis of a weight driven mechanical tower clock," in *Proceedings of the 2010 American Controls Conference*, Baltimore, MD, June 2010, pp. 634–639.
[13]E. J. Haug, *Intermediate Dynamics* (Prentice-Hall, Englewood Cliffs, NJ, 1992).
[14]J. Wagner, D. Moline, and E. Volk, "Derivation of a Seth Thomas tower clock nonlinear mathematical model," Technical Report No. TR-2011-Wagner, <myweb.clemson.edu/jwagner/archive-data>.
[15]P. Reigel, "A spring-driven No. 2? What did Seth have in mind?," NAWCC Bull. **353**, 797–800 (2004).
[16]D. A. Bateman, "Accuracy of pendulums and many factors that influence it," NAWCC Bull. **290**, 300–312 (1994).
[17]D. A. Bateman, "Pendulum timekeepers and the factors that determine their accuracy," Horological J. **132**, 83–85, 134–135, 164–165, 203–204 (1989).
[18]Analog Devices, "ADXRS150 ±150°/s single chip yaw rate gyro with signal conditioning," <www.analog.com/en/mems-sensors/mems-inertial-sensors/adxrs150/products/product.html>.
[19]Mumford Micro Systems, 3933 Antone Road, Santa Barbara, CA 93110.